Dissociative Photodetachment Dynamics of Isomeric Forms of N 3 O 2 −

ARTICLE *in* THE JOURNAL OF PHYSICAL CHEMISTRY A · MARCH 1998

Impact Factor: 2.69 · DOI: 10.1021/jp973228q

4 AUTHORS, INCLUDING:

Robert E Continetti
University of California, San Diego
128 PUBLICATIONS **2,311** CITATIONS

SEE PROFILE

Dissociative Photodetachment Dynamics of Isomeric Forms of $N_3O_2^-$

M. Sowa Resat,† V. Zengin, M. C. Garner, and R. E. Continetti*

Department of Chemistry and Biochemistry, University of California, San Diego, 9500 Gilman Drive, La Jolla, California 92093-0314

Received: October 3, 1997; In Final Form: January 6, 1998

The dissociative photodetachment of $N_3O_2^-$ at 532, 355, and 266 nm has been studied using coincident photoelectron and photofragment translational spectroscopy in a fast-ion beam. The photoelectron spectra confirm previous experimental evidence for a weakly perturbed $NO^-(N_2O)$ complex and show for the first time a broad continuum at large electron-binding energies. Translational energy release spectra exhibit both low- and high-energy-release channels, indicating that two regions of the NO−N_2O neutral potential energy surface with very different intermolecular repulsion are accessed. Photoelectron−photofragment coincidence data confirm that the high translational energy release events are correlated with the continuum in the photoelectron spectrum. These dissociative photodetachment dynamics are consistent with the existence of two isomeric species, an ion−dipole complex with the charge localized on the NO moiety and a molecular anion with an estimated stability of 2.0 ± 0.2 eV relative to NO + N_2O + e^-.

1. Introduction

Polyatomic ions can frequently exist in a variety of isomeric forms. To assess the role played by molecular and cluster ions in plasmas and other environments, it is essential to characterize the energetics and structures of potential isomers. A variety of experimental techniques including optical and photoelectron spectroscopies,[1] photodissociation and collision-induced dissociation,[2,3] and cluster reactivity studies[4] have previously been used to infer the properties of molecular and cluster anions. In this work, we report the application of photoelectron−photofragment coincidence spectroscopy to the characterization of isomeric forms of the $N_3O_2^-$ molecular ion. In these experiments photoelectron and photofragment kinetic energies are measured in coincidence to characterize the process $N_3O_2^- \rightarrow NO + N_2O + e^-$.

The dynamics of dissociative photodetachment (DPD) can provide insights into the structure of molecular anions and the dissociative states of the corresponding neutrals. Removal of an electron from an anion with a significantly different geometry from the corresponding neutral species leaves the neutral in a highly repulsive region of the potential energy surface, leading to a "direct" dissociation that is typically characterized by a large release of translational energy. This behavior is observed in the case of the DPD of O_4^-.[5] On the other hand, cluster ions bound predominantly by electrostatic interactions may not experience a significant structural distortion relative to the neutral complex. In this case photodetachment will access a weakly repulsive region of the neutral potential energy surface with a correspondingly small translational energy release between the photofragments. Dynamics consistent with this process have been observed in the DPD of $O_2^-{\cdot}H_2O$.[6] In the DPD of $N_3O_2^-$, two pathways are observed, one leading to a large translational energy release and an unstructured photoelectron spectrum and the other leading to a small translational energy release and a structured photoelectron spectrum.

There have been numerous studies of electron-induced chemistry in N_2O. Kinetic studies of electron attachment[7] and detachment processes[8] have provided important quantitative information for modeling the negative-ion chemistry of the nitrogen oxides. Moruzzi and Dakin first proposed $N_3O_2^-$ as an important species on the basis of studies of the pressure dependence of the negative-ion chemistry of N_2O.[9] Later, rate constants for the production of $N_3O_2^-$ from the three-body reaction of $NO^- + 2N_2O$ were measured by Parkes[10] and Marx et al.[11]

More recent photodetachment experiments and high-pressure mass spectrometry studies have stimulated new interest in the possible isomeric forms of $N_3O_2^-$. Using photoelectron spectroscopy, Coe et al.[12] observed spectra consistent with an ion−dipole complex $NO^-(N_2O)$. The spectrum they recorded at 514 nm (2.54 eV) is similar to the photoelectron spectrum of free NO^- showing a long vibrational progression in the neutral NO. The spectrum showed a shift to higher electron-binding energy by ≈0.22 eV. These results were interpreted as resulting from an intact NO^- core ion solvated and stabilized by N_2O. The shift in the electron affinity is primarily due to the ion−induced-dipole interaction in the anion.

Evidence for a more stable isomer, $N_3O_2^-$, has been provided by Hiraoka et al.[13] using pulsed-electron-beam high-pressure mass spectrometry to examine the equilibria of ion−molecule reactions in N_2O. Given the abundance of $N_3O_2^-$ in their room-temperature ion source, they suggested a binding energy of this species of at least ≈0.4 eV. $N_3O_2^-$ was also observed by Hayakawa et al.[14] at temperatures up to 500 K. These experimental observations suggest that this second $N_3O_2^-$ isomer is a covalently bound molecular anion. Hiraoka et al. could not obtain quantitative experimental data on the stability of $N_3O_2^-$ but performed ab initio calculations (MP2/6-31+G*//ROHF/6-31+G) that indicated the presence of both a covalently bound w-shaped O−N−N−N−O^- molecule and the ion−dipole complex $NO^-(N_2O)$, as shown schematically in Figure 1. These

* Corresponding author. Email: rcontinetti@ucsd.edu. Tel: (619)-534-5559. Fax: (619)-534-7042.

† Permanent address: Department of Chemistry, Bosphorus University, 80815 Bebek, Istanbul, Turkey.

S1089-5639(97)03228-3 CCC: $15.00
Published on Web 02/14/1998

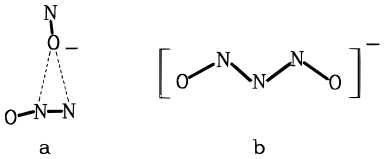

Figure 1. Structures of (a) the triplet ion−dipole $NO^-(N_2O)$ complex and (b) singlet w-shaped $N_3O_2^-$ as determined by Hiraoka et al.[13]

calculations showed that the covalent $N_3O_2^-$ is stabilized by ≈1.25 eV relative to NO + N_2O + e^-.

Motivated by Hiraoka's study of $N_3O_2^-$, Papai and Stirling recently performed density functional calculations on the stability of covalently bound neutral N_3O_2 species.[15] They found open cis, trans, and w-shaped N_3O_2 structures, with the cis isomer most stable. They note that the w-shaped isomer, found to be the most stable form of the anion by Hiraoka et al., is 0.13−0.35 eV higher in energy than *cis*-N_3O_2. It was also found that while both open and cyclic forms of N_3O_2 appear to have stable local minima, they are energetically unstable relative to NO + N_2O or N_2 + NO_2.

This paper reports experimental studies of DPD processes producing a photoelectron and two neutral fragments from $N_3O_2^-$. In these experiments, the translational energy release between the neutral photofragments is measured in coincidence with the photoelectron kinetic energy, providing a direct measure of the total translational energy released in a DPD event. This information is required to determine the stability of an ion that has Franck−Condon overlap with a repulsive region of the neutral potential energy surface. In the following sections, the experimental techniques are briefly reviewed prior to a presentation of the photoelectron, photofragment, and photoelectron−photofragment correlation spectra.

2. Experimental Section

The photoelectron-photofragment coincidence spectrometer used in these experiments has been previously described in detail,[5,16] so only a brief overview will be given here. Anions are produced in a 600-Hz pulsed free-jet expansion by electron impact on pure N_2O with a 1-keV electron beam. In the free-jet, anions at $m/e = 74$ are formed by secondary-electron-attachment processes and collisionally cooled in the expansion. The anions pass through a skimmer to enter a differentially pumped chamber where they are accelerated to an energy of 2.5−8 keV and mass-selected by time-of-flight. The high beam energy is required for efficient detection of the neutral particles produced by photodetachment. In the interaction region the ion packet is intercepted orthogonally by the linearly polarized 100-ps pulsed output of a Nd:YAG laser operating at one of three harmonic wavelengths: 532, 355, or 266 nm.[17] The laser intensities used were ≈700 MW/cm^2 at 532 nm and ≈200 MW/cm^2 at 355 and 266 nm. The laser electric vector, **E**, was rotated with respect to the beam velocity using a half-wave plate.

The laboratory kinetic energy and recoil angle of photodetached electrons are determined by time-of-flight and position-of-arrival using a large-solid-angle photoelectron detector.[18] This detector is centered above the intersection of the laser and ion beam and subtends ≈4% of the full solid angle. The photoelectron recoil angle must be measured to allow correction for the large Doppler shift produced by the fast-ion beam. The short laser pulse allows accurate electron kinetic energy measurements by time-of-flight with a nominal flight path of only 7.5 cm. Determination of the center-of-mass electron kinetic energy, eKE, fixes the energy remaining in the neutral complex. The center-of-mass electron kinetic energy resolution is ≈4% $\Delta E/E$, with an accuracy in this energy range determined by calibrations with I^- and O^- of ≈1.5%.

If the neutral species dissociates, the photofragments recoil out of the beam and impinge on a two-particle time- and position-sensitive detector. Residual anions are removed from the beam with an electrostatic deflector, allowing only stable neutrals and neutral photofragments to reach the detector. Conservation of linear momentum in the center-of-mass frame serves to determine the mass ratio of the photofragments and that they originate from a single dissociation event. Given the mass ratio, beam velocity, flight path, and the time and position of photofragment arrival, the center-of-mass translational energy release, E_T, is determined.[19] Photoelectron-photofragment coincidence is determined by counting statistics, with false coincidences estimated to be ≈5%. The resolution of the E_T measurement is <10% $\Delta E_T/E_T$, and the accuracy is ≈2%.[16] Experiments were performed at two photofragment flight paths, 0.95 and 1.95 m, and several beam energies to allow both low- and high-E_T processes to be examined.

Measurement of the translational energy release between the photofragments in coincidence with the photoelectron kinetic energy provides a direct measure of the partitioning of kinetic energy in the system, yielding a complete kinematic characterization of dissociative photodetachment events producing an electron and two neutral photofragments. Ionic photodissociation processes yielding stable ionic photofragments can also be investigated by turning off the electrostatic deflection field and recording ionic + neutral photofragments. No evidence for production of stable ionic photofragments produced in two-body dissociation was observed in these studies, although there is evidence for a three-body ionic photodissociation yielding O^-, as discussed below.

3. Results

In the following sections, the experimental results on the dissociative photodetachment

$$N_3O_2^- + h\nu \rightarrow NO + N_2O + e^-$$

are presented. First, the photoelectron spectra are shown, which yield the vertical detachment energy, i.e., the energy difference between the anion and the neutral at the anion geometry. Second, the photofragment translational energy release spectra are presented, providing a measure of the repulsive energy in the neutral relative to the operative dissociation asymptotes. Finally, the photoelectron-photofragment energy correlation spectrum at 266 nm is presented. The correlation spectrum yields both a measure of the overall dissociative photodetachment dynamics and the stability of the ion relative to the free electron and photofragments.

3.1. Photoelectron Spectra. The photoelectron spectra, N(eKE), recorded for $N_3O_2^-$ at 532 (2.33 eV), 355 (3.49 eV), and 266 nm (4.66 eV) are shown in Figure 2. These spectra were recorded by enforcing coincidence of the electron with at least one photofragment or stable neutral product. The photofragment detector was positioned for these measurements to allow any stable or low-E_T neutral products to be detected.

The photoelectron spectra at 532 and 355 nm exhibit structure similar to that reported by Coe et al.[12] at 514 nm. A vibrational progression resembling that observed for free NO^-,[20] with NO^- to NO vibrational transitions from $v'' = 0$ to $v' = 0-5$, is observed with an apparent photodetachment onset at an electron-binding energy of 0.25 eV. This is a shift of 0.22 eV to lower eKE relative to free NO. There is little change in the overall

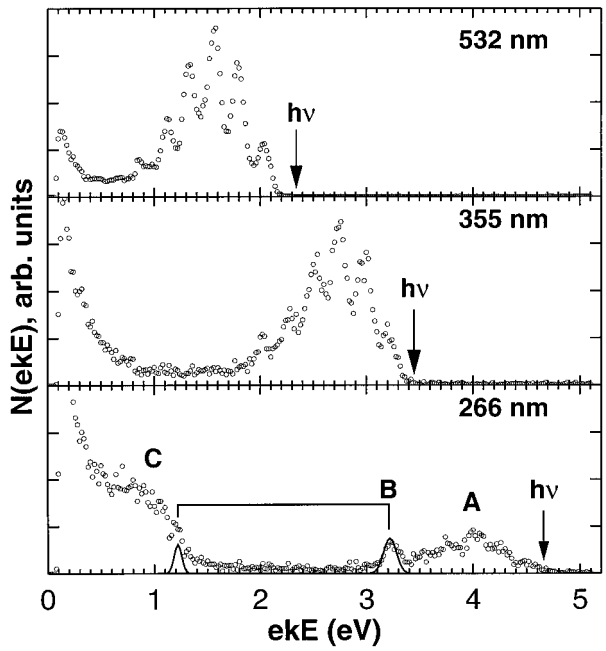

Figure 2. Photoelectron spectra, N(eKE) of $N_3O_2^-$ as a function of laser wavelength. The spectra represent the number of photoelectrons per 20-meV energy bin. The laser electric vector **E** was directed along the beam-velocity vector, and an electron was detected in coincidence with at least one heavy particle. Arrows indicate the photon energies at 532, 355, and 266 nm. The data presented for 532 nm was recorded with a beam energy of 2.5 keV, while the 355- and 266-nm data were recorded at 6 keV. The features labeled A, B, and C in the 266-nm data are discussed in the text.

Franck−Condon profile, but some broadening occurs for the individual transitions. As discussed by Coe et al., these photoelectron spectra are consistent with a weakly bound cluster ion $NO^-(N_2O)$, structure a in Figure 1. There is also a rising photoelectron signal at low energies observed in both spectra arising from background photoelectrons produced by the ion beam and scattered photons.

Increasing the photon energy to 4.66 eV reveals new features in the photoelectron spectrum (bottom frame of Figure 2). In addition to the characteristic $NO^-(N_2O)$ signal at high electron kinetic energies (A), there are two new features—a large broad shoulder at ≈0.9 eV (C) and a sharp peak and a shoulder indicated as B. The $NO^-(N_2O)$ feature (A) shows no vibrational resolution at this wavelength because of the decrease in resolution of the time-of-flight measurement for these high-energy photoelectrons. The features B at 3.2 and 1.2 eV arise from photodetachment of $O^- + h\nu \rightarrow O(^3P), O(^1D) + e^-$. This implies that O^- is produced by photon absorption at 266 nm. Because of low signal levels, it was not possible to measure the laser-fluence dependence of these features. The energetics of the broad feature (C) at 266 nm will be shown to be consistent with a single-photon dissociative photodetachment by the correlation spectra below.

3.2. Product Translational Energy Distributions. Photofragment translational energy release spectra, $N(E_T)$, were recorded at all three wavelengths. Measurement of the translational energy release at beam energies from 2.5 to 8 keV gave consistent results, indicating that $N_3O_2^-$ undergoes prompt dissociation. At these energies the flight time for $N_3O_2^-$ from the interaction region varies from 19.1 to 10.7 μs, respectively. The lack of a beam-energy-related shift in the apparent E_T provides an upper limit to the dissociation lifetime of ≈500 ns. The E_T probability distribution, $P(E_T)$, and the photofragment angular distribution, $I(\theta)$, relative to the laser **E** vector, are

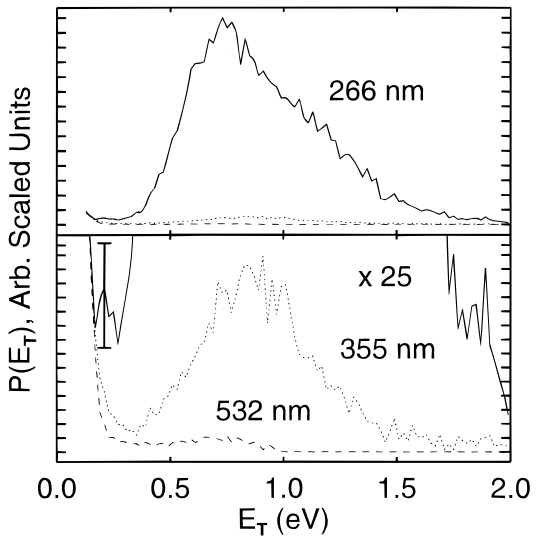

Figure 3. Product translational energy distributions, $P(E_T)$, recorded for NO + N_2O products of the dissociative photodetachment of $N_3O_2^-$ as a function of laser wavelength. The 266-nm $P(E_T)$ is shown as the solid line, 355 nm as the dotted line, and 532 nm as the dashed line. These spectra are normalized to the rising off-scale low-energy feature present in all of the data. In the lower frame, a multiplication by 25 shows the relative intensity of the data at 355 and 532 nm. A representative error bar for the $P(E_T)$ at 266 nm is shown at 0.21 eV in the lower frame.

extracted from the $N(E_T)$ with a straightforward numerical correction for the finite angular acceptance of the detector as described in refs 6, 16 and 19. The $P(E_T)$'s as a function of wavelength are shown in Figure 3. These spectra are scaled to the rising low-energy feature in the $P(E_T)$ at $E_T < 0.2$ eV, common to all three wavelengths. Photoelectron-photofragment correlation spectra show that this low-E_T feature arises from DPD of the ion−dipole $NO^-(N_2O)$ complex. As the figure indicates, the high-energy-release channel is significantly larger at 266 nm, with the integrated $P(E_T)$ in the range $0.5 < E_T < 2.0$ eV for the wavelengths 532:355:266 nm being 1.7:25:730. Owing to statistical and systematic errors in the determination of the $P(E_T)$ at low E_T, these ratios may vary by up to a factor of 5 but clearly confirm the experimental observation that the high-energy-release channel is significantly enhanced at 266 nm. Fits to the $I(\theta)$ yield the photofragment anisotropy parameter as a function of translational energy, $\beta(E_T)$. The fit (not shown) shows $\beta \approx 0.7$ near the peak of the $P(E_T)$ at all three wavelengths. This shows that DPD leading to the large E_T channel results in a rapid dissociation, with the photofragments peaked along the direction of the dipole absorption.[21]

At all three wavelengths a two-component spectrum is observed. The feature rising at $E_T < 0.1$ eV demonstrates that most neutrals dissociate with very little recoil. As the photofragment recoil decreases at low E_T, the ability to determine the photofragment mass ratio from time and position measurements decreases. At all recoil energies, however, the photofragment mass spectrum peaks at product masses of 30 amu (NO) and 44 amu (N_2O), with a full width at half-maximum of ±1 amu at $E_T > 0.3$ eV. The high-E_T peak in the spectra, at 0.7 eV in the 532-nm spectrum, moves up to 0.9 eV at 355 nm and back to 0.75 eV at 266 nm. A significant difference in the spectra involves the high-E_T tail. At 532 nm the high-E_T channel is weak, with little or no $P(E_T)$ at $E_T > 1.0$ eV. At 355 nm, the high-E_T limit moves out to $E_T \approx 1.5$ eV. At 266 nm, where the high-E_T channel is most significant, $P(E_T)$ extends beyond 2.0 eV. The presence of the high-E_T channel shows that some NO + N_2O photofragments are produced at all

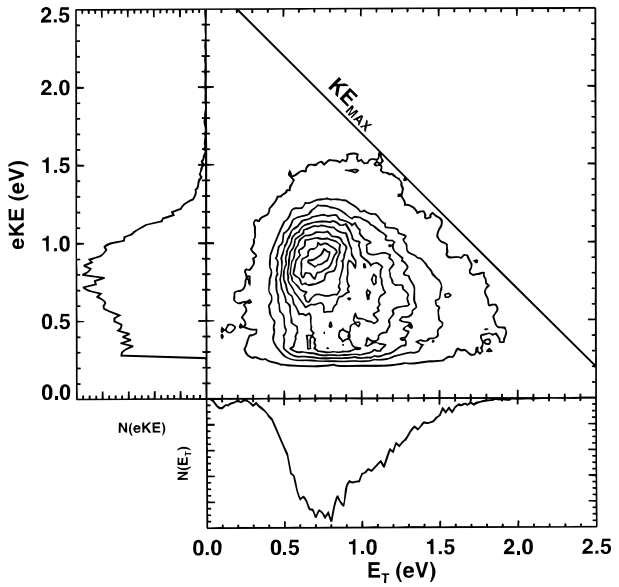

Figure 4. Correlation spectrum of the photoelectron kinetic energy with the photofragment translational energy release at 266 nm, recorded at a beam energy of 4 keV with the **E** vector parallel to the beam velocity. 19 000 triple-coincidence events are included in this 2-d histogram and smoothed with a five-point boxcar algorithm. The assigned maximum kinetic energy for the photoelectron + photofragments, $KE_{MAX} = 2.7$ eV, is shown as the solid diagonal line. The lowest contour, near KE_{MAX}, is at 2% of the peak, with the rest of the contours linearly spaced from 15% to 95%.

wavelengths with significant repulsion in the nascent neutral complex. The qualitative conclusion to be reached at this point is that photodetachment or photodissociation followed by autodetachment produces neutral species with both low and high repulsion at all wavelengths.

3.3. *N*(E_T, eKE) Correlation Spectra. Measurement of the photoelectron kinetic energy and the photofragment translational energy release in coincidence allows the overall partitioning of translational energy among the three particles to be directly measured. High signal-to-noise correlation spectra showing the origin of the high-E_T channel at 532 and 355 nm were not obtained because of the low cross section for the high-E_T channel at these wavelengths. As mentioned earlier, spectra recorded at 532 nm clearly showed the correlation of the $NO^-(N_2O)$ photoelectrons with the low-E_T channel but are not presented here. The correlation spectrum of E_T and eKE at 266 nm is shown as the contour map in Figure 4. In this spectrum, no effort has been made to correct for the photofragment and photoelectron detector energy and angular acceptance. The *y*-axis is the photoelectron spectrum, *N*(eKE), the *x*-axis shows the photofragment *N*(E_T) spectrum, and the contour map shows the correlation of E_T and eKE. The broad feature observed in the contour map shows that the broad photoelectron peak at 0.9 eV is correlated with the high-E_T peak in the *N*(E_T) spectrum. Thus, photodetachment of $N_3O_2^-$ accesses a region of the NO + N_2O neutral surface that is characterized by a significant repulsion and hence a large translational energy release. The broad low-energy feature in the photoelectron spectrum is better resolved from the laser background than in Figure 2 owing to the fact that this is three-particle coincidence data. Requiring three particles from a single event to be detected in coincidence provides increased discrimination against laser-generated photoelectron background.

The (E_T, eKE) correlation spectrum yields an estimate of the stability of covalently bound $N_3O_2^-$ relative to NO + N_2O + e^-. The total available energy is defined as the difference between the photon energy and the energy required to produce NO + N_2O + e^- at zero translational energy and in the lowest quantum states. Energy conservation dictates that DPD events are constrained to lie within a triangle formed by the eKE and E_T axes and the maximum kinetic energy of the three particles, KE_{MAX}. The contours in Figure 4 display the triangular shape dictated by energy conservation. The diagonal line drawn at the 2% contour in Figure 4 from (E_T, eKE) = (0.0, 2.7) to (2.7, 0.0) provides an estimate of KE_{MAX}. Given the photon energy of 4.66 eV, this indicates a stability of this form of $N_3O_2^-$ relative to NO + N_2O + e^- of 2.0 eV. This is an accurate measure of the stability if it is assumed that some of the NO + N_2O products are produced with no internal excitation, and the parent $N_3O_2^-$ is cold. The validity of these assumptions will be further discussed below.

4. Discussion

The results presented here illustrate the complementary nature of photoelectron and photofragment translational energy release measurements and the insights into isomeric anions that can be gained from the use of these techniques in coincidence. In particular, when a strongly bound anion has Franck−Condon overlap only with a highly repulsive region of a neutral potential energy surface, it is essential to measure both the photoelectron and photofragment translational energy release to obtain a measure of the stability of the anion relative to a free electron and the neutral products.

Both the *N*(eKE) spectra and the *P*(E_T) distributions provide evidence for the existence of at least two isomeric forms of $N_3O_2^-$. The *N*(eKE) spectra at 532 and 355 nm support the solvated NO^- interpretation given by Coe et al.[12] $NO^-(N_2O)$ is a weakly bound ion−dipole complex in which the excess charge resides largely on the NO. The resulting photoelectron spectra closely parallel that of free NO, with a stabilization of 0.22 eV upon solvation. The observation of the broad photoelectron signal at 266 nm (peak C in Figure 2) is indicative of a different form of the anion. The occurrence of other photodestruction processes is also shown by the observation of the O^- photoelectron spectrum at 266 nm.

Translational spectroscopy of the photofragments yields two important pieces of information. Determination of the photofragment mass ratio identifies the dissociation products. In addition, the translational energy released in dissociation provides a measure of the repulsion in the nascent neutral. Consider photodetachment of the ion−dipole complex $NO^-(N_2O)$. Given the small solvation energy in the cluster ion inferred by Coe et al.,[12] little nuclear rearrangement and thus little repulsive energy is expected in the photodetached neutral complex. In this case, the energy released in translation between the NO + N_2O photofragments is expected to be small, consistent with the significant low-E_T channel observed at all wavelengths. In addition, a high-E_T channel is also observed at all wavelengths. In the absence of further information, this indicates that a fraction of the NO + N_2O molecules are produced with significant repulsive energy or that energy transfer from internal degrees of freedom to photofragment translation occurs in the dissociation.

The strongest evidence for the covalent $N_3O_2^-$ anion is provided by the 266-nm N(E_T, eKE) correlation spectrum in Figure 4. The broad photoelectron peak at eKE = 0.9 eV is shown to be correlated with the high-E_T channel in this spectrum. The absence of extensive structure in the eKE spectrum could be a result of transitions between low-frequency vibrational modes in the anion and the neutral. Given that the

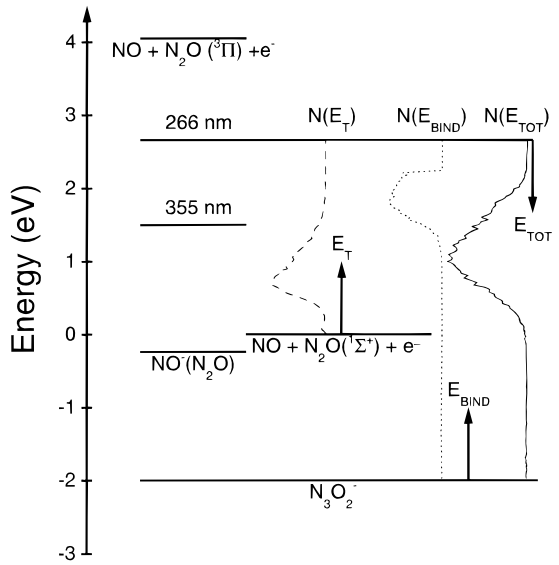

Figure 5. Energetics of the dissociative photodetachment of $N_3O_2^-$. $NO + N_2O + e^-$ is shown as the zero of energy. $NO^-(N_2O)$ is shown at -0.24 eV,[12] and the experimental stability of $N_3O_2^-$ is shown at -2.0 eV. The vertical short-dashed spectrum shows the photoelectron spectrum at 266 nm as the electron-binding energy relative to $N_3O_2^-$, $N(E_{BIND})$. The vertical long-dashed spectrum shows $N(E_T)$ at 266 nm, with $E_T = 0$ at $NO + N_2O + e^-$. Finally, the vertical solid-line spectrum shows the 266-nm total translational energy spectrum, $N(E_{TOT})$, plotted with $E_{TOT} = 0$ at the 266-nm photon energy. The 355- and 266-nm photon energies are shown relative to $N_3O_2^-$. The origin and direction of increasing energy for each spectrum is indicated by the arrows.

photoelectrons are observed to be correlated with the high-E_T channel, however, the simplest explanation for this feature is direct dissociative photodetachment on a repulsive surface.

Figure 5 summarizes the data obtained on the stability of $N_3O_2^-$ in these experiments. The covalent form, $N_3O_2^-$, is placed at -2.0 eV relative to the $NO + N_2O + e^-$ dissociation asymptote. The photon energies for 355- and 266-nm photodetachment are plotted relative to this $N_3O_2^-$ origin. The E_T spectrum at 266 nm provides a measure of the photofragment repulsion and is plotted with $E_T = 0$ at the $NO + N_2O + e^-$ dissociation asymptote. The 266-nm photoelectron spectrum is plotted as the photoelectron binding energy, $E_{bind} = E_{h\nu} -$ eKE, showing directly the vertical excitation of $\approx$3.9 eV required to reach the repulsive state of N_3O_2 from $N_3O_2^-$. This shows that Franck−Condon overlap with the repulsive state of N_3O_2 is greatest at $\approx$1.9 eV above $NO + N_2O + e^-$. The signal in the 266-nm photoelectron spectrum extends below the 355-nm photon energy, indicating that the repulsive state can also be accessed by photodetachment at 355 nm. Finally, the total translational energy release spectrum at 266 nm, obtained from the correlation spectrum by binning $E_{TOT} =$ eKE $+ E_T$ for each event, is shown plotted with $E_{TOT} = 0$ at the 266-nm photon energy. This shows that the coincidence data is consistent with the DPD of $N_3O_2^-$: $N_3O_2^- + h\nu \rightarrow NO + N_2O + e^-$.

As discussed above, the correlation spectrum indicates that $N_3O_2^-$ is bound by 2.0 eV relative to $NO + N_2O + e^-$. For this to be an accurate value requires two conditions: cold $N_3O_2^-$ and production of at least some ground-state $NO + N_2O$ products. Concerning internal excitation in the parent $N_3O_2^-$, given that the ion source also produces the weakly bound $NO^-(N_2O)$ species, it is safe to assume that low-frequency vibrational degrees of freedom are cooled in the supersonic expansion. High-frequency modes, however, will be less efficiently cooled. With the triatomic molecules O_3^- [22] and CCO^- [23] stretching mode hot bands consistent with vibrational temperatures of 450−1100 K have been found with this source. Concerning the second condition, significant internal excitation in the photoproducts is expected. Hiraoka's[13] most stable calculated geometry for the covalent $N_3O_2^-$ finds the N_2O moiety to be bent by 115.5°. Upon dissociation, N_2O becomes linear, resulting in a photoproduct with substantial excitation in the bending mode at $\approx$590 cm^{-1},[24] in addition to other internal degrees of freedom in NO and N_2O. Examination of the E_{TOT} spectrum in Figure 5 shows some signal extending $\approx$0.2 eV below $NO + N_2O + e^-$. If it is assumed that none of this is due to vibrational excitation in the anion, the stability of $N_3O_2^-$ would have to be *decreased* to 1.8 eV relative to $NO + N_2O + e^-$. Similarly, if no ground-state fragments are produced, no signal is observed at the true maximum E_{TOT}. This would also require a *decrease* in the stability of $N_3O_2^-$. If vibrational excitation in excess of 0.2 eV in the anion appears in product (electron or photofragment) kinetic energy, an *increase* in the stability of $N_3O_2^-$ would be required. Owing to these uncertainties, the stability of $N_3O_2^-$ is reported as 2.0 eV, with an estimated error of $\pm$0.2 eV.

An unexplained aspect of the DPD of $N_3O_2^-$ is the weak high-E_T channel observed at 532 nm. There are several possible explanations for this process. One involves vibrational-to-translational energy transfer in the $NO(v)-N_2O$ neutral complex. To peak at 0.7 eV, transfer of three vibrational quanta to translation would need to be the dominant process, which appears to be unlikely at the relatively low vibrational excitation of $NO(v \leq 6)$ produced in photodetachment.[25] A second possibility is a third isomer, with the charge localized on the N_2O. On the basis of the 0.22-eV adiabatic electron affinity of N_2O,[26] the N_2O^-(NO) species is expected to be more stable than $NO^-(N_2O)$. N_2O^-(NO) is more difficult to form, however, since a substantial barrier must be overcome to attach an electron to N_2O. While N_2O is linear, N_2O^- is predicted to be bent, with an N−N−O bond angle of $\approx$134°.[27] The energy required to bend the neutral to 134° is estimated to be 1 eV,[27] which may channel into photofragment translation upon photodetachment of an N_2O^-(NO) isomer. Because of the large geometry difference between N_2O and N_2O^-, there is poor Franck−Condon overlap between the lowest energy levels in the ion and neutral, and any photoelectrons produced in photodetachment of N_2O^-(NO) would be expected to be distributed over a broad energy range, as observed by Coe et al. in N_2O^- and $(N_2O)_2^-$.[28] This would make observation of this isomer in the photoelectron spectra difficult, so it cannot be ruled out. Photodissociation of $N_3O_2^- \rightarrow NO^-(v > 0) + N_2O$, followed by rapid autodetachment of the vibrationally excited NO^-, may also contribute to a high-E_T channel. As shown in our previous work on $O_4^- \rightarrow O_2^-(v > 3) + O_2$,[29] in such cases it may be possible to observe electrons at specific eKE corresponding to specific $NO^-(v'') \rightarrow NO(v') + e^-$ transitions. Electron-scattering studies have shown that autodetachment of NO^- occurs with small changes in vibrational state,[30] however, so such electrons would be at low eKE and hard to detect. Further studies of the weak high-E_T channel at 532 nm are required.

An additional process to consider in the photochemistry of $N_3O_2^-$ is ionic photodissociation. The observation of features associated with the photodetachment of O^- in the 266-nm photoelectron spectrum shows that ionic photodissociation occurs at this wavelength. Free NO^- does not photodissociate at this wavelength, and no evidence for two-body photodissociation producing stable ionic products was seen in the $N(E_T)$ photofragment spectra at any wavelength. Thus, production of O^- must occur by a three-body dissociation. Considering the

possible products of the photodissociation at 266 nm, an energetically favorable reaction is the three-body dissociation process: $N_3O_2^- + h\nu \rightarrow N_2 + NO + O^-$. This reaction has been previously discussed as a source of O^- from the reaction $NO^- + N_2O$ by Gorden and Ausloos.[31]

Whether this photodissociation occurs on a repulsive ionic surface or perhaps via photoassisted dissociative electron attachment (DEA) to N_2O[32] remains to be determined. Photoassisted DEA might occur in the ion−dipole complex when the electron photodetached from NO attaches to the nearby N_2O molecule, leading to the well-known dissociative attachment reaction $N_2O + e^- \rightarrow N_2 + O^-$. It is unclear, however, why this channel would only be observed at 266 nm, as the cross section for dissociative attachment to free N_2O peaks at an electron energy of 2.5 eV.[33] Photodetached electrons at an energy of ≈2.5 eV are most efficiently produced at 355 nm, where no evidence for the O^- channel has been observed. It is possible, however, that the nearby NO perturbs the energy dependence of the dissociative attachment cross section.

Finally, a comparison of the experimental result on the stability of $N_3O_2^-$ with the calculations of Papai and Stirling[15] on neutral N_3O_2 can be made. They found the w-shaped form of N_3O_2 to be ≈1.3 eV higher in energy than $NO + N_2O$, and while the open cis form of N_3O_2 was a local minimum, the w-shaped isomer is a transition state. These results are qualitatively consistent with the energetics as shown in Figure 5. As discussed earlier, the photoelectron spectrum at 266 nm indicates that the photodetachment process yields states of N_3O_2 ≈1.9 eV above $NO + N_2O$. These experiments showed no evidence for the production of stable N_3O_2 produced by photodetachment of $N_3O_2^-$. The failure to observe evidence for stable states of N_3O_2 in the photoelectron spectra may be due to either a lack of Franck−Condon overlap with bound regions of the N_3O_2 potential energy surface or the absence of long-lived states of N_3O_2.

5. Conclusion

These experiments demonstrate that there are at least two forms of $N_3O_2^-$ produced in the electron-impact free-jet ion source: the ion−dipole complex and a more stable molecular anion. DPD of the ion−dipole complex $NO^-(N_2O)$ is observed to lead to small translational energy release (<0.1 eV), while DPD of the covalently bound complex leads to a translational energy release peaking at $E_T \approx 0.8$ eV between the NO and N_2O photoproducts. Coincident measurement of photoelectron and photofragment kinetic energies in dissociative photodetachment provides an experimental value of 2.0 ± 0.2 eV for the stability of $N_3O_2^-$ relative to $NO + N_2O + e^-$. Evidence is also observed for a three-body ionic photodissociation process, most likely producing $O^- + N_2 + NO$. We are currently constructing an apparatus capable of examining this and other three-body dissociations that should provide a more complete picture of the dissociation dynamics of the $N_3O_2^-$ anion. These results show that photoelectron-photofragment coincidence spectroscopy can be a valuable tool for providing information on the structure, energetics, and dynamics of isomeric molecular and cluster anions.

Acknowledgment. This work was supported by the Air Force Office of Scientific Research under Grant F49620-96-1-0220. R.E.C. is a Camille Dreyfus Teacher−Scholar and acknowledges the support of a 1994 Packard Fellowship in Science and Engineering. We acknowledge helpful discussions with Drs. K. A. Hanold, R. Dressler, and A. A. Viggiano.

References and Notes

(1) Castleman, A. W.; Bowen, K. H. *J. Phys. Chem.* **1996**, *100*, 12911.
(2) Lifshitz, C. In *Cluster Ions*; Ng, C. Y., Baer, T., Powis, I., Eds.; John Wiley: New York, 1993; pp 121−164.
(3) Bastian, M. J.; Dressler, R. A.; Levandier, D. J.; Murad, E.; Muntean, F.; Armentrout, P. B. *J. Chem. Phys.* **1997**, *106*, 9570.
(4) Anderson, S. L. In *Clusters of Atoms and Molecules II;* Haberland, H., Ed.; Springer-Verlag: Berlin, 1994; pp 241−259.
(5) Hanold, K. A.; Garner, M. C.; Continetti, R. E. *Phys. Rev. Lett.* **1996**, *77*, 3335.
(6) Sherwood, C. R.; Continetti, R. E. *Chem. Phys. Lett.* **1996**, *258*, 171.
(7) Caledonia, G. E. *Chem. Rev. (Washington, D.C.)* **1975**, *75*, 333.
(8) Viggiano, A. A.; Morris, R. A.; Paulson, J. F. *J. Phys. Chem.* **1990**, *94*, 3287.
(9) Moruzzi, J. L.; Dakin, J. T. *J. Chem. Phys.* **1968**, *49*, 5000.
(10) Parkes, D. A. *J. Chem. Soc., Faraday Trans. 1* **1972**, *68*, 2103.
(11) Marx, R.; Mauclaire, G.; Fehsenfeld, F. C.; Dunkin, D. B.; Ferguson, E. E. *J. Chem. Phys.* **1973**, *58*, 3267.
(12) Coe, J. V.; Snodgrass, J. T.; Freidhoff, C. B.; McHugh, K. M.; Bowen, K. H. *J. Chem. Phys.* **1987**, *87*, 4302.
(13) Hiraoka, K.; Fujimaki, S.; Aruga, K.; Yamabe, S. *J. Phys. Chem.* **1994**, *98*, 8295.
(14) Hayakawa, S.; Matsumoto, A.; Yoshioka, M.; Matsuoka, S.; Sugiura, T. *Mass. Spectrosc.* **1986**, *34*, 147.
(15) Papai, I.; Stirling, A. *Chem. Phys. Lett.* **1996**, *253*, 196.
(16) Sherwood, C. R.; Hanold, K. A.; Garner, M. C.; Strong, K. M.; Continetti, R. E. *J. Chem. Phys.* **1996**, *105*, 10803.
(17) Xie, X.; Simon, J. D. *Opt. Commun.* **1989**, *69*, 303.
(18) Hanold, K. A.; Sherwood, C. R.; Garner, M. C.; Continetti, R. E. *Rev. Sci. Instrum.* **1995**, *66*, 5507.
(19) Continetti, R. E.; Cyr, D. R.; Osborn, D. L.; Leahy, D. J.; Neumark, D. M. *J. Chem. Phys.* **1993**, *99*, 2616.
(20) Siegel, M. W.; Celotta, R. J.; Hall, J. L.; Levine, J.; Bennett, R. A. *Phys. Rev. A* **1972**, *6*, 607.
(21) Zare, R. N. *Mol. Photochem.* **1972**, *4*, 1.
(22) Garner, M. C.; Hanold, K. A.; Sowa Resat, M.; Continetti, R. E. *J. Phys. Chem. A* **1997**, *101*, 6577.
(23) Zengin, V.; Persson, B. J.; Strong, K. M.; Continetti, R. E. *J. Chem. Phys.* **1996**, *105*, 9740.
(24) Huber, K. P.; Herzberg, G. *Molecular Spectra and Molecular Structure III. Electronic Spectra of Polyatomic Molecules*; Van Nostrand: New York, 1966; p 596.
(25) Yang, X.; Price, J. M.; Mack, J. A.; Morgan, C. G.; Rogaski, C. A.; McGuire, D.; Kim, E. H.; and Wodtke, A. M. *J. Phys. Chem.* **1993**, *97*, 3944.
(26) Hopper, D. G.; Wahl, A. C.; Wu, R. L. C.; Tiernan, T. O. *J. Chem. Phys.* **1976**, *65*, 5474.
(27) Ferguson, E. F.; Fehsenfeld, F. C.; Schmeltekopf, A. L. *J. Chem. Phys.* **1967**, *47*, 3085.
(28) Coe, J. V.; Snodgrass, J. T.; Freidhoff, C. B.; McHugh, K. M.; Bowen, K. H. *Chem. Phys. Lett.* **1986**, *124*, 274.
(29) Li, R. J.; Hanold, K. A.; Garner, M. C.; Luong, A. K.; Continetti, R. E. *Discuss. Faraday Soc.* **1998**, *108*, in press.
(30) Schulz, G. J. *Rev. Mod. Phys.* **1972**, *45*, 423.
(31) Gorden, R.; Ausloos, P. *J. Res. Natl. Bur. Stand.* (*U.S.*) **1965**, *69A*, 79.
(32) Parnis, J. M.; Hoover, L. E.; Pedersen, D. B.; Patterson, D. D. *J. Phys. Chem.* **1995**, *99*, 13528.
(33) Chantry, P. J. *J. Chem. Phys.* **1969**, *51*, 3369.